Available online at www.sciencedirect.com

ScienceDirect

Procedia Engineering 2 (2010) 825–833

Procedia Engineering

www.elsevier.com/locate/procedia

Fatigue 2010

Effect of pin tool thread orientation on fatigue strength of friction stir welded AZ31B-H24 Mg butt joints

S.M. Chowdhury[a], D.L. Chen[a*], S.D. Bhole[a], X. Cao[b]

[a]*Department of Mechanical and Industrial Engineering, Ryerson University, 350 Victoria Street, Toronto, Ontario M5B 2K3, Canada*
[b]*Aerospace Manufacturing Technology Centre, Institute for Aerospace Research, National Research Council Canada, 5145 Decelles Avenue, Montreal, Quebec H3T 2B2, Canada*

Received 17 February 2010; revised 10 March 2010; accepted 15 March 2010

Abstract

The aim of this investigation was to evaluate the fatigue resistance of friction stir welded (FSWed) AZ31B-H24 Mg alloy butt joints with emphasis on the effect of pin tool thread orientation (right-hand thread (RHT) and left-hand thread (LHT)) in the clockwise rotation. The friction stir welding resulted in recrystallized grains in the stir zone (SZ) and thermomechanically-affected zone (TMAZ), and partially recrystallized grains in the heat-affected zone (HAZ), with the lowest hardness appeared in the SZ. The fatigue life after friction stir welding was observed to be lower at high stress amplitudes, but remained nearly the same at low stress amplitudes. Fatigue strength was higher in the FSWed joints made with the LHT pin tool than with the RHT pin tool due to the elimination of the welding defects near the bottom surface via a downward material flow. Fatigue fracture basically occurred at or near the boundary between TMAZ and SZ. Fatigue crack initiated from the specimen surface or near surface defects in the case of LHT pin tool, and from the welding defects near the bottom surface in the case of RHT pin tool. Crack propagation was characterized by the formation of fatigue striations.

Keywords: Magnesium alloy; friction stir welding; microstructure; fatigue strength; pin tool thread orientation.

1. Introduction

The transportation industry is facing a significant challenge in reducing the weight of vehicles to improve fuel economy and reduce greenhouse gas emissions without compromising safety and reliability. The reduction of vehicle weight is best achieved via combining the use of lightweight materials with innovative structural design. Magnesium alloys have attracted special attention of researchers and engineers especially working in the transportation industry because they are the lightest structural metallic materials with high specific strength and stiffness, good heat conductivity, high electromagnetic interference shielding and damping capabilities, good machinability and castability [1-4]. However, effective joining techniques are required in the structural applications of magnesium alloys. Friction stir welding (FSW), a solid state joining technique invented by The Welding Institute in Cambridge, England nearly two decades ago [5], has been termed as “green” technology by many researchers due to its energy efficiency and environment friendliness. The development and application of FSW technology in lightweight structures in the aerospace, automotive and shipbuilding industries provide an effective tool of achieving

* Corresponding author. Tel: +1 416 979 5000 ext. 6487; fax: +1 416 979 5265. E-mail address: dchen@ryerson.ca (D.L. Chen).

1877-7058
doi:10.1016/j.proeng.2010.03.089

superior joint integrity especially where reliability and damage tolerance are of major concerns [6]. Since the automotive and aerospace components are inevitably subjected to dynamic or cyclic stresses in services, the fatigue properties of the friction stir welded (FSWed) joints must be properly evaluated to ensure the safety and longevity.

During FSW frictional heat generated between the cylindrically threaded pin and shoulder and the work-pieces causes the material to soften (without reaching its melting point), and the plasticized material is rapidly stirred/mixed to form the FSWed joint. This would cause a big change in the material microstructure and/or flow pattern, and subsequent mechanical properties of the joint, depending on the FSW parameters and pin tool geometry. Colligan [7] reported the material flow pattern of a FSWed Al alloy obtained using a stop action technique with a left hand screw threaded pin tool in a clockwise rotation, and observed that the stirred material was forced down in the weld by the threads on the pin and is deposited in the weld nugget. Later Guerra *et al.* [8], and Zhao *et al*. [9] made FSWed joints using right hand thread (counterclockwise) tool profile, while Schnider and Nunes [10] used left hand thread (clockwise) tool profile and observed no occurrence of welding defects. The combination of the thread orientation with the rotation of the pin tool increased an extra downward force and heat generation that would be beneficial to accelerate the flow of plasticized material to ensure good mechanical bonding. On the other hand, Cao and Jahazi [11] recently observed some noticeable defects at the bottom or root of the welded joints with a right hand screw threaded pin in the clockwise rotation. These observations indicated that the material flow pattern during FSW is a function of pin tool thread and direction of rotation. But little is known of the effect of the left hand thread (LHT) and right hand thread (RHT) pins on the microstructure and fatigue properties of the FSWed Mg alloy. The objective of this study was, therefore, to evaluate the dependence of fatigue resistance on the pin tool thread orientation in a FSWed AZ31B-H24 Mg alloy in relation to its microstructural change.

Nomenclature

σ_a	cyclic stress amplitude
σ_f'	fatigue strength coefficient
N_f	number of cycles to failure
$2N_f$	number of reversals to failure
b	fatigue strength exponent

2. Experimental procedures

In the present study a 2 mm thick AZ31B-H24 Mg alloy sheet was selected. The nominal composition of this alloy was 2.5-3.5 wt% Al, 0.7-1.3 wt% Zn, 0.2-1.0 wt% Mn and balance Mg [11]. Prior to FSW, surface oxide layers were removed with a steel brush and then the surface was cleaned using ethanol. Butt welding was conducted without additional filler metal. Two welding parameters were changed: the welding speed (10 and 30 mm/s) and tool rotational rate (1000 and 2000 rpm) by using a LHT pin in the clockwise rotation. To observe the effect of thread orientation both LHT and RHT pins were employed at a welding speed of 10 mm/s and tool rotational rate of 2000 rpm in a clockwise rotation. The welded work-pieces were cut in the direction perpendicular to the welding direction to examine the cross-sectional microstructure. Then the specimens were cold mounted, ground, polished and etched with acetic picral (10 mL acetic acid (99%), 4.2 g picric acid, 10 mL H_2O, 70 mL ethanol (95%)) [11]. An optical microscope coupled with Clemex image analysis system was used to observe the microstructural change across the welds. Fatigue tests were conducted using a fully computerized Instron 8801 servo-hydraulic testing system under load control at different stress amplitudes. At each stress level at least two samples were tested. A stress ratio of R ($\sigma_{min}/\sigma_{max}$) equal to 0.1, sinusoidal waveform, and frequency of 50 Hz were selected in all the tests. After the fatigue

tests the base metal and the welded joints were examined via a JSM-6380LV scanning electron microscope (SEM) equipped with Oxford energy dispersive X-ray spectroscopy (EDS) system and 3D fractographic analysis, to identify fatigue crack initiation sites and propagation mechanisms.

3. Results and discussion

3.1. Microstructure and microhardness profiles

All the FSWed joints in this investigation were observed using optical microscope at a magnification of 1000× to examine the quality of FSWed regions. Fig. 1 shows a typical example of the cross section of the FSWed sample made at a welding speed of 10 mm/s and tool rotational rate of 1000 rpm including base metal (BM), heat-affected zone (HAZ), thermo-mechanically affected zone (TMAZ) and stir zone (SZ). The retreating side (RS) and advancing side (AS) are indicated in Fig. 1(a). The microstructure of the AZ31B-H24 Mg BM consisted of pancake-shaped grains with varying sizes (Fig. 1(b)). The heterogeneity in the grain structure of the BM was due to both deformation of the 2 mm thick sheet by rolling and incomplete dynamic recrystallization during partial annealing [11]. The average grain size of the BM was about 3.6±2.2 μm. Both equiaxed and elongated grains were observed in the HAZ as shown in Fig. 1(c). The presence of some equiaxed grains observed in the HAZ indicated that partial recrystallization had taken place. Fig. 1(d) presents the microstructure of the TMAZ, where the recrystallized grains were basically observed. In the SZ fully recrystallized grains appeared (Fig. 1(d)). These microstructural changes across the FSWed Mg alloy joint were similar to those reported in [12].

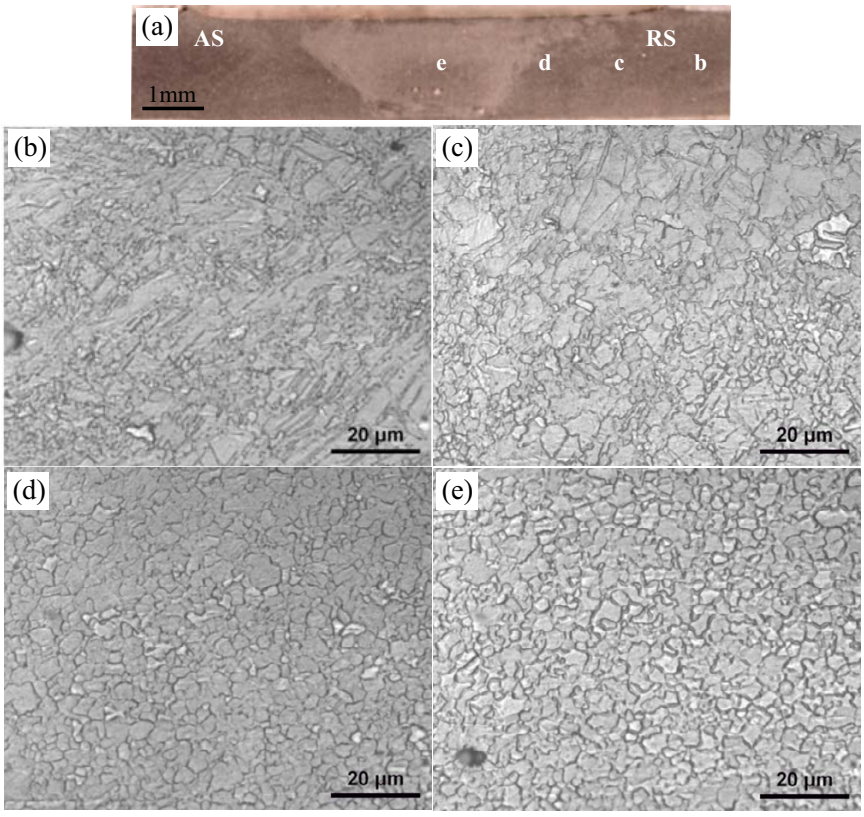

Fig. 1. (a) Microstructures of a FSWed joint obtained at a welding speed of 10 mm/s and tool rotational rate of 1000 rpm; (b) base metal; (c) heat-affected zone (HAZ); (d) thermomechanically-affected zone (TMAZ); and (e) stir zone (SZ).

Mg alloys would experience dynamic recrystallization more easily than Al alloys because the recrystallization temperature of Mg alloys was about 523K [13] which was generally lower than that of Al alloys. During FSW, the peak temperature experienced in these regions (SZ, TMAZ) was higher than the recrystallization temperature of the Mg alloy, so that the deformed microstructure just outside the SZ would also be dynamically recrystalllized. This would be the main reason why the TMAZ possessed a similar microstructure to that in the SZ in AZ31B-H24 Mg alloy. It was observed that grain size became smaller by increasing welding speed from 10 mm/s to 30 mm/s and decreasing tool rotational rate from 2000 rpm to 1000 rpm. This was due to the fact that the heat input decreased with increasing welding speed and decreasing rotational rate [12,14]. Furthermore, less time was available for grain growth at a higher welding speed.

The microhardness profile is shown in Fig. 2 at a welding speed of 10 mm/s and a rotational rate of 1000 rpm. It is seen that the hardness values decreased gradually from about HV73 in the half-hard H24 temper BM to approximately HV63 at the center of the SZ through the HAZ and TMAZ of the welded joint. The hardness in the SZ varied from 87% to 90% of the BM hardness when the tool rotational rate decreased from 2000 rpm to 1000 rpm while the welding speed remained constant at 10 mm/s. The decrease in the hardness would be partially correlated to the grain growth, in addition to the change of the material state from the H24 temper to recrystallzation state. Similar changes in the microstructure and the resulting hardness were reported in [12,15].

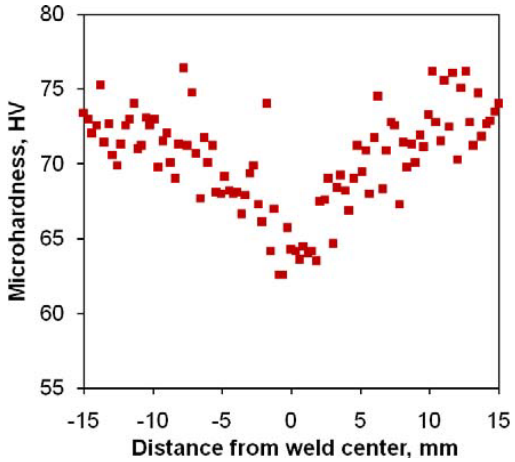

Fig. 2. Typical microhardness profile of a FSWed sample at a welding speed of 10 mm/s and a rotational rate of 1000 rpm.

3.2. Fatigue behavior

Load controlled fatigue tests were conducted on both the BM and the FSWed specimens and the obtained results are shown in Fig. 3. It is seen that at high stress amplitudes all the FSWed joints had a lower fatigue life than the BM. As the stress amplitude decreased the difference of fatigue life between the FSWed joints and the BM became smaller at low stress amplitudes. The fatigue limit of the FSWed joints made with LHT pin was about 20% lower than that of the BM, whereas the fatigue limit of the FSWed joints made with RHT pin was 40% lower than that of the BM. The obtained fatigue limit (defined as the fatigue strength corresponding to 1×10^7 cycles) and fatigue ratio (the ratio of the fatigue limit to the ultimate tensile strength) of the FSWed joints are listed in Table 1. While the absolute value of fatigue limit was lower, the fatigue ratio of the FSWed joints using LHT pin tool was higher than that of the BM, with the lowest fatigue ratio obtained for the FSWed joints using RHT pin tool.

The following Basquin-type equation [16] could be used to fit the fatigue data,

$$\sigma_a = \sigma_f'(2N_f)^b, \tag{1}$$

where σ_a is the alternating stress amplitude, σ_f' is the fatigue strength coefficient defined by the stress intercept at $2N_f$ =1, N_f is the number of cycles to failure and $2N_f$ is the number of reversals to failure, and b is the fatigue strength exponent. The obtained σ_f' and b values are listed in Table 2.

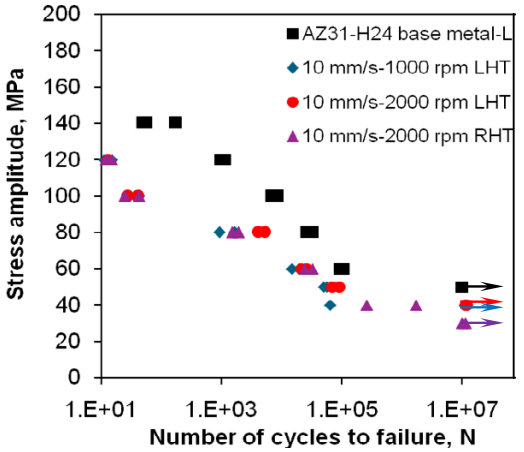

Fig. 3. S-N curves of the AZ31B-H24 base metal in the longitudinal direction, and FSWed joints at a welding speed of 10 mm/s and rotational rate of 1000 and 2000 rpm using LHT and RHT pin tools.

Table 1. Fatigue limit and fatigue ratio of the FSWed joints.

Welding parameter	Pin thread orientation	Fatigue limit (MPa)	Tensile strength (MPa)	Fatigue ratio
Base metal	-	50	285	0.175
10 mm/s and 1000 rpm	LHT	40	212	0.190
10 mm/s and 2000 rpm	LHT	40	211	0.190
10 mm/s and 2000 rpm	RHT	30	207	0.145

Normally a smaller value of b corresponded to a longer fatigue life [16]. From Table 2 it can be seen that the absolute value of the fatigue strength exponent for the FSWed joints using RHT pin tool was a little larger than that for the FSWed joints using LHT pin tool, thus corresponding to a shorter fatigue life, as also seen in Fig. 3. This was mainly due to the presence of some welding defects at or near the bottom surface of the FSWed joints using RHT pin tool. Fatigue life was indeed associated with both fatigue strength exponent and fatigue strength coefficient based upon equation (1). The longer fatigue life of the base metal shown in Fig. 3 was apparently related to a considerably (1.7~1.8 times) higher fatigue strength coefficient in spite of its higher absolute value of fatigue strength exponent.

Table 2. Fatigue strength coefficient σ_f' and fatigue strength exponent b of the FSWed joints.

Welding parameter	Pin thread orientation	σ_f' (MPa)	b
Base metal		274	-0.115
10 mm/s and 1000 rpm	LHT	149	-0.086
10 mm/s and 2000 rpm	LHT	154	-0.089
10 mm/s and 2000 rpm	RHT	160	-0.093

To understand the effect of the pin thread orientation on the fatigue behavior of the FSWed joints, it is necessary to analyze the flow pattern of the material during FSW. Nunes *et al.* [17] synthesized a model of flow around the nib

(or pin) out of (1) a pure transition flow field; (2) a rigid disc rotation flow field; (3) a radially symmetrical vortex ring flow field (inward at the shoulder, down at the nib threads, outward on the lower part of the nib, and upwards in the outer regions around the nib) to simulate the material circulation during FSW. Then they pointed out that clockwise and counterclockwise welds (with the same pin tool) would have opposing directions of vortex circulation. Based on their model a 2-dimensional material flow pattern around the nib during FSW could be schematically plotted in Fig. 4. It is seen that the use of RHT and LHT pin tools resulted in a reversal of material flow, where the softened material very close to the RHT pin tool flew upward while the material in the vicinity of the LHT pin tool flew downward. It has been reported that the pin should be threaded and rotated in such a manner that the material should be pushed down by the threads (for example, a RHT pin tool turning counterclockwise) to achieve good welded joints [10]. As a result, in the present study the LHT pin tool in the clockwise rotation (Fig. 4(b)) would give rise to better joints while the RHT pin tool in the clockwise rotation (Fig. 4(a)) would result in the occurrence of potential porosity or lack-of-bonding defects due to two possible reasons. First, the FSW was considered to be a constant volume welding process and the upward material movement would cause the plasticized material to stick to shoulder and pin [18], which would reduce the supply of plasticized material at the bottom. Second, due to a certain extent of temperature gradient between the top surface in contact with the shoulder and bottom surface in touch with the clamping support [19], the material flow near the bottom surface would encounter more flow resistance when it flew upward. Therefore, the welds obtained using the RHT pin in the clockwise rotation had increasing probability to form porosity or lack-of-bonding defects near the bottom surface. Such defects were clearly seen from the fracture surface after fatigue testing of the FSWed joints made with the RHT pin tool in the clockwise rotation (Fig. 5(a)), while no such defects were observed in the FSWed joints made with the LHT pin tool in the clockwise rotation (Fig. 5(b)). The metallographic observations or fractographic examinations after tensile testing of the FSWed joints made with the RHT pin tool revolving clockwise showed the presence of porosity and lack-of-bonding defects as well [11,20]. Therefore, the lower fatigue limit or fatigue life of the FSWed joints made with the RHT pin tool rotating clockwise (Fig. 3 and Table 1) was attributed to the presence of the porosity and lack-of-bonding defects near the bottom surface.

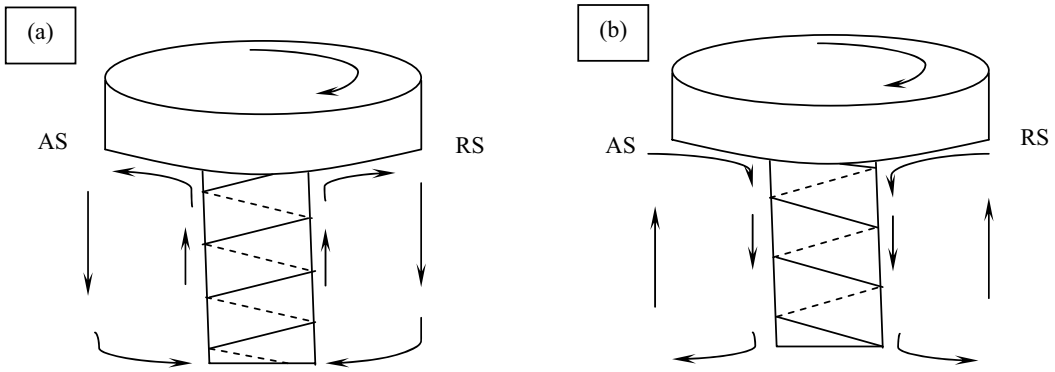

Fig. 4. Effect of pin thread orientation on the material flow around the pin during FSW, (a) RHT; (b) LHT.

All the welded joints of the Mg alloy failed at or near the boundary between TMAZ and SZ. The failure locations of the FSWed joints are listed in Table 3. It is seen that failure location was sensitive to the thread orientation of the pin that was related to the material flow pattern during FSW. The FSWed joints obtained using the LHT pin failed at the AS, while the FSWed joints obtained using the RHT pin failed mainly at the RS. According to Zhao *et al*. [9] the material flowed from the AS to the RS, and went around the pin and back to the AS again. During FSW, some materials were lost and thus the AS which was the farthest place to be filled would have a higher risk to form porosity, leading to the failure in the AS. For the FSWed joints obtained using the RHT pin, the failure which mainly appeared at the RS was apparently due to the reversal of the material flow direction (Fig. 4(a)).

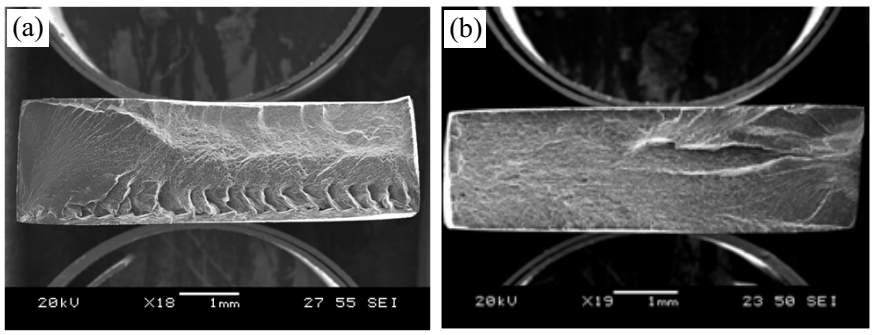

Fig. 5. SEM images showing the fracture surfaces of the FSWed samples, after fatigue testing at a stress amplitude of 60 MPa, made with (a) RHT pin tool; (b) LHT pin tool in the clockwise rotation.

Table 3. Failure location of the FSWed specimens during fatigue testing.

Welding parameter	Pin tool thread orientation	Failure location	
		Advancing side (AS)	Retreating side (RS)
10 mm/s and 1000 rpm	LHT	11	0
10 mm/s and 2000 rpm	LHT	11	0
10 mm/s and 2000 rpm	RHT	2	8

3.3 Fractography

Fig. 6 shows typical SEM images taken from the fracture surface of a FSWed sample made with the LHT pin tool in the clockwise rotation at a stress amplitude of 60 MPa. Fatigue crack initiation basically occurred either from the defects or unmelted particles present at the specimen surface as shown in Fig. 5 and Fig. 6(a). The presence of an Al-Mn particle was responsible for the initiation during fatigue testing as shown in Fig. 6(b), (c) and (e). For the FSWed samples made with the RHT pin tool in the clockwise rotation fatigue crack initiation was observed to initiate from the bottom surface welding defects, since the lack-of-bonding defects or pores could act as a stress raiser, facilitating the crack initiation. Fatigue crack propagation was basically characterized by fatigue striations (Fig. 6(d)), which were usually perpendicular to the propagating direction with the spacing increased with increasing distance from the initiation site. While the fatigue striations normally occurred by a repeated plastic blunting-sharpening process in the face-centered cubic materials due to the slip of dislocations in the plastic zone ahead of the fatigue crack tip, the formation of the fatigue striations in the magnesium alloys was expected to be related to the twinning in the compressive phase and detwinning in the tensile phase [3,21-23]. Further studies are needed in this aspect.

Conclusions

1. The FSW of AZ31B-H24 Mg alloy resulted in recrystallized grains in the SZ and TMAZ, and partially recrystallized grains in the HAZ. The lowest hardness values were obtained at the center of the FSWed joints.
2. Fatigue strength or life was observed to be higher in the FSWed joints made with the LHT pin tool in the clockwise rotation than that of the FSWed joints made with the RHT pin tool in the same rotational

direction. This was due to the elimination of the welding porosity located near the bottom surface of the FSWed joints in the former case via a downward material flow close to the pin tool surface.

3. While the FSW resulted in a lower fatigue life at high stress amplitudes, the fatigue limit (or strength at low stress amplitudes) of the FSWed joints made with the LHT pin tool in the clockwise rotation was only slightly lower than that of the BM.
4. Fatigue fracture basically occurred at or near the boundary between TMAZ and SZ in either AS or RS, depending mainly on the pin tool thread orientation. It appeared that the use of RHT pin tool in the clockwise rotation promoted the failure at the RS.
5. Fatigue crack initiation occurred from the specimen surface or near surface defects in the FSWed joints made with the LHT pin tool, and from the welding defects near the bottom surface in the FSWed joints made with the RHT pin tool in the clockwise rotation. In all cases fatigue crack propagation was characterized by the formation of fatigue striations with the spacing increased with increasing distance from the initiation site.

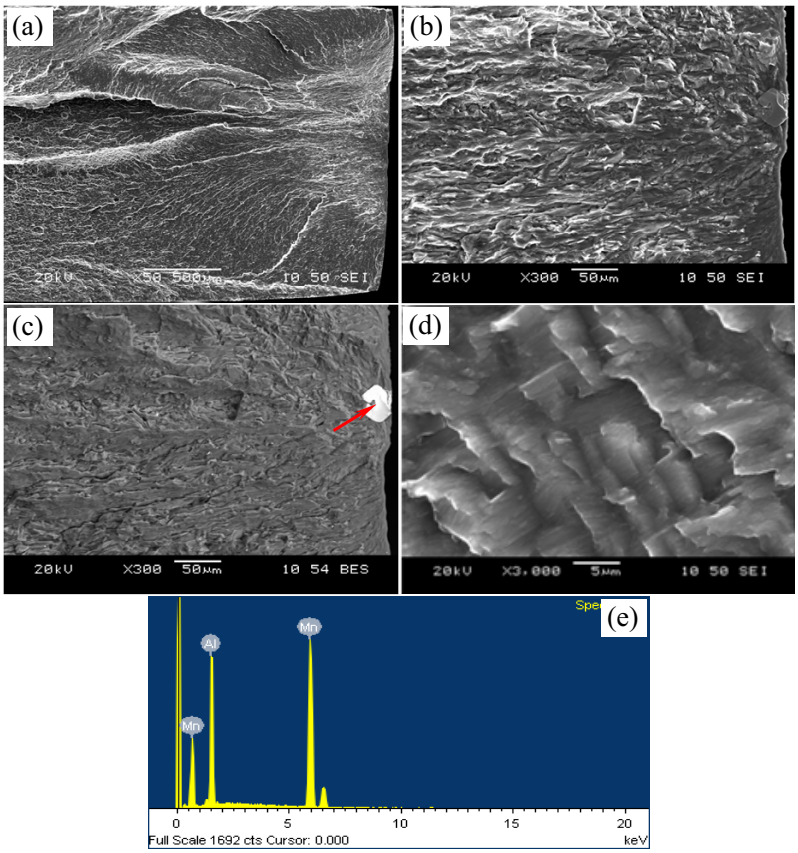

Fig. 6. Typical SEM images of the fatigue fracture surface of a FSWed sample made with the LHT pin tested at a stress amplitude of 60 MPa. (a) fatigue crack initiation area at a low magnification; (b) fatigue crack initiation area at an intermediate magnification; (c) backscattered electron image of (b); (d) fatigue crack propagation area at a high magnification; (e) EDS spectrum of the particle near the surface on the image (c) indicated by an arrow.

Acknowledgements

The authors would like to thank the Natural Sciences and Engineering Research Council of Canada (NSERC) and AUTO21 Network of Centers of Excellence for providing financial support. This investigation involves part of Canada-China-USA Collaborative Research Project on the Magnesium Front End Research and Development (MFERD). The authors also thank General Motors Research and Development Center for the supply of test materials. One of the authors (D.L. Chen) is grateful for the financial support by the Premier's Research Excellence Award (PREA), Canada Foundation for Innovation (CFI), and Ryerson Research Chair (RRC) program. The authors would like to thank Q. Li, A. Machin, J. Amankrah, D. Ostrom and R. Churaman (Ryerson University) and M. Guerin (Aerospace Manufacturing Technology Centre, NRC) for their assistance in the experiments. The authors also thank Dr. S. Xu, Dr. K. Sadayappan, Dr. J. Jackman, Professor N. Atalla, Professor N. Zhou, Professor D. Weckman, Professor S. Lambert, Professor H. Jahed, Professor Y.S. Yang, Professor B. Jordon, Dr. A.A. Luo, Mr. R. Osborne, Dr. X.M. Su, and Mr. L. Zhang for the helpful discussion.

References

[1] Essadiqi E. Magnesium sheet technology perspectives. *JOM* 2009;**61**:13–3.

[2] Nyberg EA, Luo AA, Sadayappan K, Shi WF. Magnesium for future autos. *Adv Mater Processes* 2008;**166**:35–7.

[3] Begum S, Chen DL, Xu S, Luo AA. Effect of strain ratio and strain rate on low cycle fatigue behavior of AZ31 wrought magnesium alloy. *Mater Sci Eng A* 2009;**517**:334–43.

[4] Tsujikawa M, Somekawa H, Higashi K, Iasaki H, Hasegawa T, Mizuta A. Fatigue of welded magnesium alloy joints. *Mater Trans* 2004;**45**:419–22.

[5] Thomas WM, Nicholas ED, Needham JC, Murch MG, Templesmith P, Dawes CJ. GB Patent Application No.9125978.8. December 1991.

[6] Lomolino S, Tovo R, dos Santos J. On the fatigue behaviour and design curves of friction stir butt-welded Al alloys. *Inter J Fatigue* 2005;**27**:305–16.

[7] Colligan K. Material flow behavior during friction stir welding of aluminum. *Welding J* 1999;**78**:229–37.

[8] Guerra M, Schmidt C, McClure JC, Murr LE, Nunes AC. Flow patterns during friction stir welding. *Mater Characterization* 2003;**49**:95–101.

[9] Zhao Y, Lin S, Wu L, Qu F. The influence of pin geometry on bonding and mechanical properties in friction stir weld 2014 Al alloy. *Mater Lett* 2005;**59**:2948–52.

[10] Schneider JA, Nunes Jr AC. Characterization of plastic flow and resulting microtextures in a friction stir weld. *Metall Mater Trans* B 2004;**35**:777–83.

[11] Cao X, Jahazi M. Effect of welding speed on the quality of friction stir welded butt joints of a magnesium alloy. *Mater Design* 2009;**30**:2033–42.

[12] Afrin N, Chen DL, Cao X, Jahazi M. Microstructure and tensile properties of friction stir welded AZ31B magnesium alloy. *Mater Sci Eng A* 2008;**472**:179–86.

[13] Park SHC, Sato YS, Kokawa H. Effect of micro-texture on fracture location in friction stir weld of Mg alloy AZ61 during tensile test. *Scripta Mater* 2003;**49**:161–66.

[14] Lombard H, Hattingh DG, Steuwer A, James MN. Optimising FSW process parameters to minimize defects and maximize fatigue life in 5083-H321 aluminium alloy. *Eng Fract Mech* 2008;**75**:341–54.

[15] Lee WB, Yeon YM, Jung SB. Joint properties of friction stir welded AZ31B-H24 magnesium alloy. *Mater Sci Technol* 2003;**19**:785–90.

[16] Dieter GE. *Mechanical Metallurgy*. SI Metric ed. UK: McGraw-Hill Book Co; 1988.

[17] Nunes Jr AC, Bernstein EL, McClure JC. A rotating plug model for friction stir welding. Paper presented at the 81st American Welding Society Annual Convention. Chicago, IL; April 26-28, 2000.

[18] Seidel TU, Reynolds AP. Visualization of the material flow in AA2195 friction-stir welds using a marker strain technique. *Metal Mater Trans A* 2001;**32**:2879–84.

[19] Fairman M, Afrin N, Chen DL, Cao XJ, Jahazi M. Microstructural evaluation of friction stir processed AZ31B-H24 magnesium alloy. *Can Metall Quarterly* 2007;**46**:425–32.

[20] Chowdhury SM, Chen DL, Bhole SD, Cao X, Powidajko E, Weckman DC, Zhou Y. Tensile properties and strain hardening behavior of double-sided arc welded and friction stir welded AZ31B magnesium alloy. *Mater Sci Eng A* 2010;doi:10.1016/j.msea.2010.01.031.

[21] Begum S, Chen DL, Xu S, Luo AA. Strain-controlled low-cycle fatigue properties of a newly developed extruded magnesium alloy. *Metall Mater Trans A* 2008;**39**:3014–26.

[22] Wu L, Jain A, Brown DW, Stoica GM, Agnew SR, Clausen B, Fielden DE, Liaw PK. Twinning-detwinning behavior during the strain-controlled low-cycle fatigue testing of a wrought magnesium alloy ZK60A. *Acta Mater* 2008;**56**:688–95.

[23] Lou XY, Li M, Boger RK, Agnew SR, Wagoner RH. Hardening evolution of AZ31B Mg sheet. *Inter J Plast* 2007;**23**:44–86.